Book of Tutorials and Abstracts

European
Microbeam Analysis Society

University of BRISTOL

Mineralogical Society

EMAS 2018

13th EMAS Regional Workshop

MICROBEAM ANALYSIS IN THE EARTH SCIENCES

4 - 7 September 2018

University of Bristol, Wills Hall, Bristol, Great Britain

Organised in collaboration with:
Mineralogical Society of Great Britain and Ireland
and
University of Bristol

SEM ELEMENT MAPPING: STRENGTHS, LIMITATIONS AND APPLICATIONS TO PETROGRAPHY OF VOLCANIC ROCKS

D. Muir

Cardiff University, School of Earth and Ocean Sciences
Main Building, Cardiff CF10 3AT, Great Britain
e-mail: muird1@cardiff.ac.uk

Dr Duncan Muir is Senior Electron Microbeam Specialist in the School of Earth and Ocean Sciences at Cardiff University, UK. He specialises in scanning electron microscope chemical analysis including large area element mapping, quantitative energy-dispersive X-ray spectroscopy (EDS) and wavelength dispersive spectroscopy (WDS), electron backscatter diffraction (EBSD) and μ-XRF. Prior to managing the Electron Microbeam Facility, Duncan was a researcher focusing on igneous petrology and volcanology of arc systems.

Duncan graduated with a BSc (Hons) in Geology from Edinburgh University in 2004. Following a few years working in industry in the fields of mineral exploration and offshore geotechnics, in 2009 he completed an MSc in Natural Hazards at the University of Bristol. For his thesis he investigated the petrological and textural variations in lavas and domes from eruptions of Mount St. Helens volcano between 1980 and 2004. Much of this work relied upon energy-dispersive X-ray spectroscopy element mapping of groundmass crystals and glasses and subsequent phase identification and segmentation. Duncan then went on to complete a PhD at the University of Bristol using experimental petrology to study the magma storage conditions beneath Volcán Uturuncu, a dormant but actively uplifting volcano in the Bolivian Andes. During this period, Duncan gained further experience with scanning electron microscopy, electron probe microanalysis and secondary ion mass spectroscopy. He was subsequently employed as a postdoctoral research assistant at Uppsala University, Sweden where he investigated along-arc petrological variations in Sumatran volcanic rocks as well as helping to run the EMPA laboratory.

ABSTRACT

Pre-eruptive magma processes can be investigated through groundmass crystal textures of volcanic rocks. Crystal size distributions (CSD) are a means of quantifying textural data and can provide insights into crystallisation kinetics. Traditionally, backscattered electron images from scanning electron microscopes (SEM) are used to image groundmass crystals which are then segmented manually by tracing crystal outlines. This is labour intensive and commonly limits investigations to a single crystal phase. With the onset of silicon drift detectors in energy-dispersive X-ray spectrometers it has become much quicker to acquire X-ray element maps using the SEM. Here we show how such maps can be used to generate textural data by classifying each pixel as a crystal, glass or vesicle based on chemical composition. This method enables all phases to be segmented and enables concurrent acquisition of multiphase CSD, crystallinity and mineral mode data. We apply the method to 17 samples erupted from Mount St Helens, USA during the 1980 to 1986 eruptive period. Variations in CSD intercepts (n^0, nucleation density) and slopes (characteristic length or $G\tau$, the product of growth rate (G) and residence time (τ)), crystallinity and mineral modes are used to show differences in pre-eruptive magma processes between volcanic rocks (pumices, cryptodomes and domes) from summer 1980 and post-summer 1980.

1. INTRODUCTION

Magmas are made up of crystals, melt and bubbles of exsolved gas. As magmas ascend through the crust they crystallise and the texture of erupted volcanic rocks record a crystallisation history that can be related to eruption dynamics. Scanning electron microscopy (SEM) imaging has been used for decades to investigate and quantify textures of arc volcanic rocks. Most studies rely upon backscattered electron (BSE) images with manual segmentation and thresholding of crystal outlines from greyscale images. This is time consuming and often plagioclase is the only mineral reported being the most abundant in arc volcanic rocks. Phase segmentation from BSE images can be complicated as phases with similar mean atomic number e.g., albite and glass (quenched melt) or amphibole and clinopyroxene may have similar greyscale intensities leading to misidentification. Advances in energy-dispersive X-ray spectroscopy (EDS) efficiency has enabled chemical mapping of larger areas of samples over shorter time periods. Here we show how EDS element maps can be used to quantify textures in volcanic rocks from Mount St Helens, USA, in addition to providing crystallinity and mineral mode data. We relate the textural data to changes in the pre-eruptive magma system beneath the volcano during the 1980 to 1986 eruptive period.

1.1. SEM-EDSX-ray

Scanning electron microscope energy-dispersive spectroscopy (SEM-EDS) provides multispectral data recording all X-ray energies greater than approximately 100 eV up to the beam energy limit (usually 15 to 20 kV). In SEM-EDS an entire X-ray spectrum typically made up of 2048 channels is acquired with characteristic X-rays forming peaks associated with specific elements and an X-ray continuum that forms a background which scales with mean atomic number. By scanning the beam over a 2D area, a matrix of spectra can be measured forming an X-ray spectral image (XSI; Fig. 1). A spectrum can be reconstructed from each pixel of an XSI or, alternatively, the intensity of a chemical element can be viewed at multiple x-y locations over the mapped area.

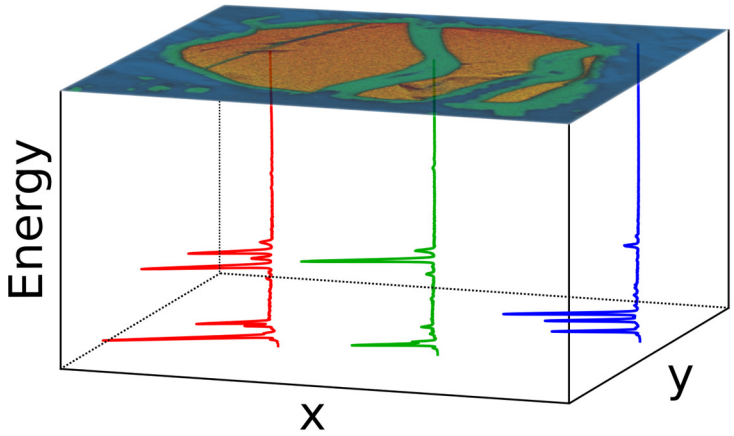

Figure 1. Schematic example of an X-ray spectral image. Full spectra of intensities can be extracted from individual pixels or relative intensities of each element present can be viewed as a map.

The first semi-conductor based EDS spectrometers used lithium-compensated silicon detectors (Si(Li)). Si(Li)-EDS performance was limited by the throughput of the Si(Li)-detector [1], which restricts the measured X-ray count rate. This was particularly problematic for mapping where high count rates with short dwell times were required as only a few hundred to a few thousand counts were acquired in each pixel spectrum. The advent of the silicon drift detector (SDD) enabled significant advances in SEM-EDS element mapping. The SDD uses similar detection physics as the Si(Li)-EDS but has an internal charge collection field with a pattern of nested electrodes on the back face. This makes it more efficient with greater throughput without compromising spectral resolution. Newbury and Ritchie [2] compare performance of a Si(Li)- and a SDD-detector with the same active area of 10 mm^2. They show that a spectral resolution of 129 eV can be achieved at Mn-Kα with an amplification time of 400 ns compared to 35 µs for Si(Li) at the same conditions. Furthermore, the throughput of the SDD

(140,000 counts per second (cps)) is around 70 times faster than the Si(Li) (1,900 cps). Another benefit of the SDD is that arrays of detectors can be created with combined active areas reaching 600 mm^2 at the time of writing.

Innovations in electron sources occurred at the same time as SDD-EDS with the commercial availability of thermal field emission gun (tFEG) electron sources. The combination of this brighter, higher beam current (typically 1 nA to 100 nA), and more stable beam with the more efficient SDD meant a step-change in EDS capabilities with regards to element mapping. Variation in beam current – a common issue over long time periods with unstable electron sources such as tungsten filaments – was largely eliminated with the tFEG which remains stable over periods of hours and days. The high count rates possible with SDDs mean element maps can now be acquired more quickly with better data quality. An entire thin-section (25 by 45 mm) can be mapped within a few hours at a step size of 20 μm using 300 mm^2 SDD-EDS with a dwell time of 5 ms.

1.2. Strengths and weaknesses of SEM-EDS

SEM-EDS is widely used to measure major and minor elements in geological samples as an alternative to using wavelength-dispersive X-ray spectroscopy (WDS) on electron microprobes (EPMA). EDS has inferior spectral resolution compared to WDS (~130 eV versus ~10 eV respectively on Mn-Kα) and has a higher detection limit (few 1,000s ppm for EDS compared to 10s to 100s ppm for WDS). Most elements can be analysed by both techniques although H and He are excluded due to lack of X-rays and Li, Be and B are difficult or even impossible to measure depending on the detector due to low X-ray energies and negligible X-ray yield. Both techniques are non-destructive and have a similar spatial resolution being of the order of 1 - 2 μm^3 at 20 kV in most silicate minerals.

Compared to EPMA-WDS, SEM-EDS is relatively cheap to install and run and remains relatively stable for long time periods once calibrated with high degrees of reproducibility. SEM-EDS chemical analyses are also quick and simple to perform with acquisition times of 10s of seconds. Consequently, large quantities of chemical data can be acquired with limited user knowledge. This is both a strength and weakness. Acquisition software algorithms are able to automatically identify elements present in concentrations above a few tenths of a weight percent. However, it is fundamental that the identified elements are verified by the operator. EDS spectra are also affected by artefacts such as pulse pile-ups, which occur when multiple X-rays arrive at the detector simultaneously and cannot be discriminated as separate signals by the pulse processor, and escape peaks caused by excitation of a Si-Kα X-rays within the detector. The X-ray contribution of the background must also be subtracted from characteristic peaks to see true variations in intensities of any particular element rather than background fluctuations.

1.3. Volcanic rock textures

The number, size and shape of crystals in a volcanic rock reflect the relative rates of nucleation and growth, which are in turn dependent on the magma solidification history as it travels to the surface. In a closed system, nucleation defines the number of crystals and growth determines each crystal size. Nucleation of a given phase at a given pressure and temperature is favoured by high levels of undercooling (ΔT) or supersaturation of a melt relative to the liquidus temperature [3] (Winkler, 1947) e.g., during rapid ascent; and growth predominates at lower ΔT e.g., during effusive, dome-building eruptions (Fig. 2). Quantification of crystal textures in groundmass of volcanic rocks from well characterised eruptions enables us to investigate pre-eruptive magmatic processes and their temporal variations.

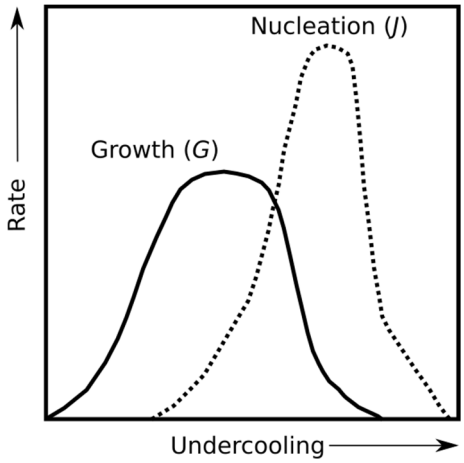

Figure 2. Relationship between undercooling (ΔT) and crystal nucleation and growth. Nucleation dominates at high degrees of undercooling. Growth is favoured at low degrees of undercooling. Figure reproduced from Cashman and Blundy [4].

Crystal size distributions (CSD) are a means of quantifying crystal contents as a function of size. Traditionally CSDs are presented as a semi-logarithmic plot of population density (n, mm^{-4}) versus apparent crystal size (L, mm). Nuclei population density (n^0, mm^{-4}) is determined from the y-intercept and characteristic crystal length ($G\tau$) is measured from the slope ($-1/G\tau$, mm^{-1}). From $G\tau$ growth rate (G, mm day^{-1}) can be estimated assuming an appropriate residence time (τ, days) or vice versa.

Past eruptions of Mount St. Helens, USA have been recorded in detail (summarised in Scott *et al.* [5]) and therefore provide a natural laboratory to study the effects of varying eruptive styles on crystal textures. Here we focus on variations in groundmass textures during the eruptive period from summer 1980 to 1986. Summer 1980 eruptions were largely explosive whilst post-summer 1980 eruptions were mostly effusive dome-building eruptions. Samples from the 18 May 1980 Plinian eruption are excluded as they do not contain microlites. Samples from a

cryptodome that formed in March 1980 are the earliest sample included and eruptions are temporally referenced to an earthquake swarm on 17 March 1980, which is widely believed to mark the initial significant ascent of magma beneath Mount St. Helens [6].

We performed element mapping of groundmass-rich regions of erupted samples to investigate the textural and petrological variations throughout the specified eruptive period. We demonstrate how quantitative textural, crystallinity and mineral mode data can be extracted from element maps providing insights into pre- and syn-eruptive processes.

2. METHODS

Thin sections of 17 Mount St. Helens dacitic volcanic rocks erupted on known dates were selected for study from existing collections at the University of Bristol. The thin sections were coated with 20 nm carbon and groundmass-rich regions devoid of phenocrysts and vesicles were identified using backscattered electron (BSE) images. Element maps of selected areas were then acquired using a tungsten filament Hitachi S-3500N scanning electron microscope with a 10 mm^2 Thermo Noran silicon drift detector energy-dispersive X-ray spectrometer (SDD-EDS). Maps were acquired at 20 kV with a step size of 1.2 μm, a dwell time of 20 ms and an amplification time of 4 μs. The dead time was approximately 30 % and count rates of 16,000 cps to 24,000 cps were achieved resulting in approximately 400 counts per pixel. A 1024 by 800 pixel X-ray spectral image (XSI) was acquired in approximately 7 hours covering a 1.2 mm^2 area of each sample.

Element maps of the relative proportions of Al, Ca, Fe, K, Mg, P, Si and Ti were extracted from the XSIs. These data were then converted to binary (black and white) phase maps using simple IF/AND/OR mineral-specific algorithms written in MATLAB with each pixel being identified as a particular mineral, vesicle or glass. Plagioclase, orthopyroxene, clinopyroxene, hornblende, olivine, iron-titanium oxides, apatite and silica phases were identified and thresholded according to relative abundances of mapped elements (e.g., Fig. 3). Vapour-phase cristobalite was identified by its cracked appearance in BSE images, and is chemically distinguished from quartz by its lower Si concentration. Chemical distinctions are particularly useful for phases with similar mean atomic number. High Al and Ca and low K content were used to distinguish plagioclase from glass and the mafic silicate phases of clinopyroxene, orthopyroxene and hornblende are identified from relative abundances of Al, Ca, Fe and Mg. Vesicles are identified as areas of low Si, Ca and/or Fe compared with crystalline or glassy areas.

Using element maps results in far higher numbers of groundmass plagioclase crystals being identified and measured compared to manual plagioclase segmentation from BSE images. For example, in sample SH135, 1,790 plagioclase crystals were thresholded from the element map

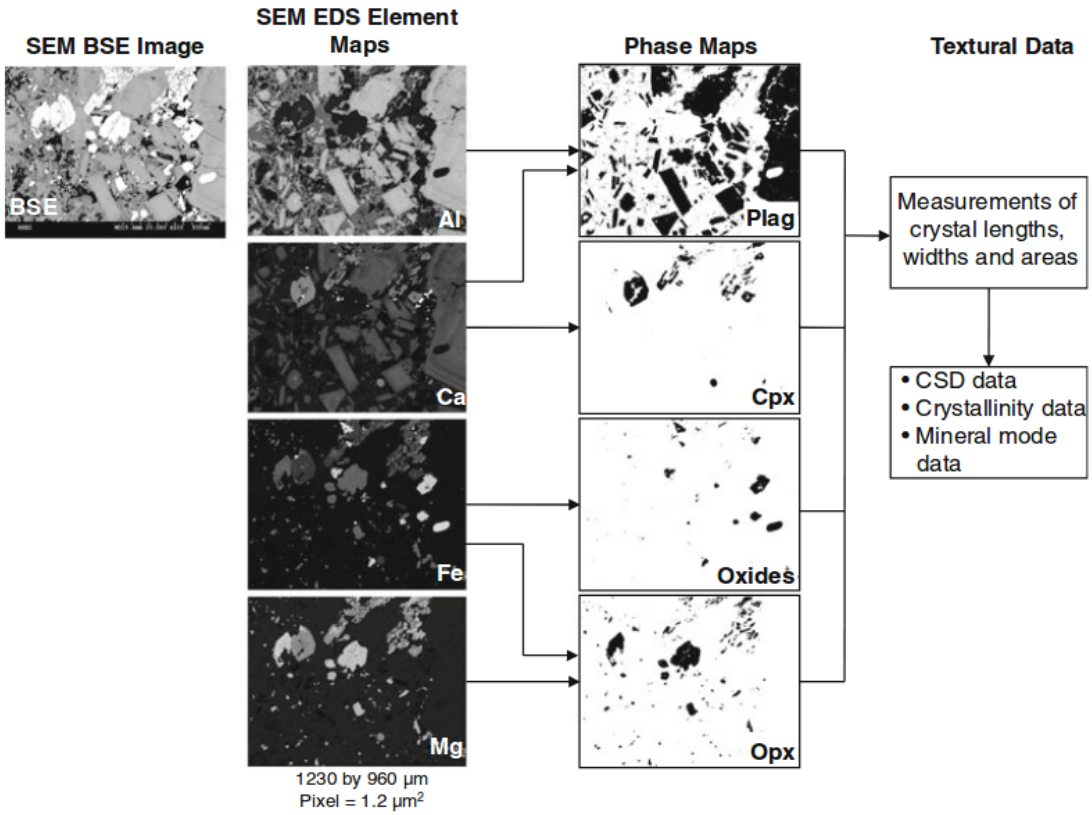

Figure 3. Illustration of how combinations of element intensities from EDS-SEM maps can be used to identify and delineate various phases as binary images. Crystal size, crystallinity and mineral mode data can be extracted from these binary images. Figure from Muir *et al.* [7].

compared with only 530 when measured manually from a BSE image of the same area. Numerous plagioclase crystals smaller than 15 µm were unidentified in the BSE image. The size of segmented phases vary slightly depending on the threshold values used to differentiate each phase. To evaluate the accuracy of the method, binary phase maps were overlayed on BSE images of the same area as a qualitative visual check. More objective, statistically based methods of extracting textural data from element maps are described in Buse and Kearns [8].

Prior to measuring particle dimensions, images were visually scanned for touching or otherwise conjoined crystals and such crystals were separated digitally. Similarly, isolated portions of resorbed crystals (e.g., hornblende in dacite) that were obviously once part of a complete, fresh crystal were reunited and treated as one to prevent overestimates of crystal numbers. Groundmass crystallinities and mineral modes were calculated from binary images for each sample using the "Measure Particles" function in ImageJ software [9].

In this study apparent crystal size (L, mm), that is, the size of a crystal in the plane of the section, is defined as the long axis of the smallest elliposoid fit. CSDCorrections (version 1.3.9; [10]) was used to correct for crystal shape and geometry in the conversion of L to a

3D crystal shape for CSD calculation. Mean aspect ratios of plagioclase and orthopyroxene with L>3 μm were calculated using CSDSlice [11]. A ratio of 1.0:1.4:2.9 was used for plagioclase and 1.0:1.3:2.0 for orthopyroxene. Each phase map was processed twice: once with crystals intersecting the image edge excluded for CSD calculations, and again with these crystals included for mineral mode calculations.

3. RESULTS AND DISCUSSION

3.1. MSH CSD results

Between 260 and 2,700 plagioclase crystals and 10 to 250 orthopyroxene crystals were thresholded from a 1.2 mm^2 area of groundmass for each sample. Crystals smaller than 5 μm are excluded from calculations of CSDs as they can cannot be imaged as accurately as larger crystals. The low abundance of orthopyroxene is problematic as the minimum number of crystals required for a statistically reliable size distribution is approximately 250 [11]. As a result, here we mostly concentrate on plagioclase CSD data. Several samples, notably pumices from summer 1980 which experienced rapid shallow ascent at high degrees of undercooling, have insufficient groundmass crystals to produce a reliable CSD from a single thin section.

Traditionally, CSDs are plotted as $ln(n)$ versus L . In this format, a simple system with initial nucleation followed by continuous growth will plot as a straight line. However, all CSDs in this study are curved and best-fit by two linear regressions for crystals smaller than 50 μm (microlites) and larger than 50 μm (microphenocrysts), respectively (Fig. 4). Curved CSDs can result from mixing of crystal populations as well as varying rates of growth in the magma system or continuously accelerating nucleation and growth [12]. Curvature can also occur by crystal compaction, crystal accumulation or fractionation and resorption.

Nuclei population densities are high at the beginning of the 1980 eruption ($ln(n^0) = 18.85 \pm 0.20$ mm^{-4}) but decrease sharply during summer 1980 to $ln(n^0) = 15.53 \pm 0.16$ mm^{-4} before increasing gradually overall during post-summer 1980 dome-building eruptions (Fig. 5). Summer 1980 CSDs typically have higher n^0 than post-summer 1980 eruptive products probably because ascent rate, and therefore ΔT, decreased post-summer 1980 promoting growth of pre-existing crystals. However, $G\tau$ of plagioclase microlites are similar during and post-summer 1980 (mean = 8.3 ± 1.7 μm and mean = 8.8 ± 1.3 μm, respectively). For samples with sufficient orthopyroxene microlites, mean $G\tau$ is 11.0 ± 1.1 μm either indicating faster growth rates or longer residence times for orthopyroxene in the system. The number of orthopyroxene microlites remains approximately constant throughout the eruption with increasing crystallinity mostly occurring as a result of crystal coarsening.

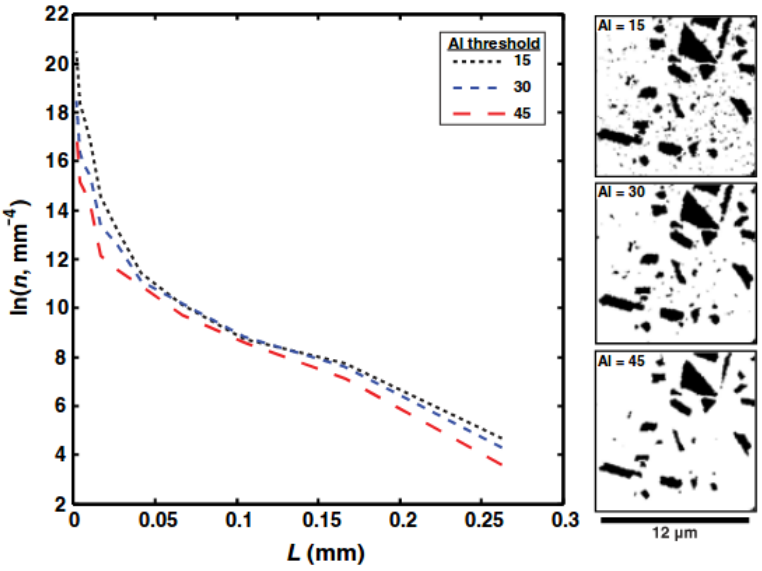

Figure 4. Examples of plagioclase CSDs for SH156-2 erupted 17 June 1984 produced from crystal measurements from a binary image. Varying thresholds of Al in terms of counts intensity has the demonstrated impact on CSD data. Figure from Muir *et al.* [7].

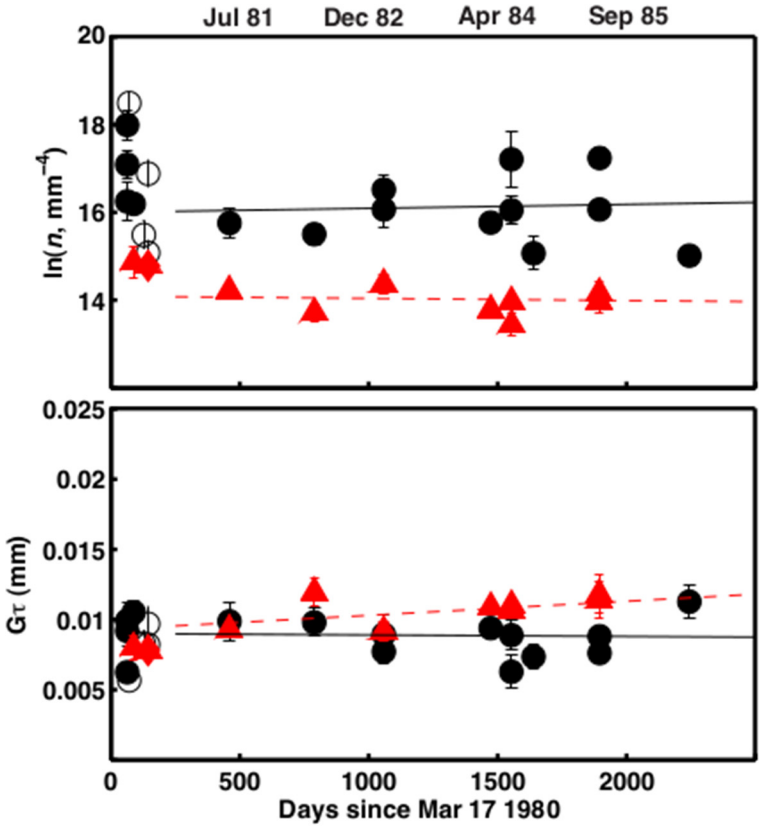

Figure 5. Variation of n^0 and $G\tau$ with time since the March 17 1980 earthquake swarm. Black circles are plagioclase microlites, red triangles are orthopyroxene microlites. Open symbols are pumices and filled symbols are cryptodomes or domes. Figure from Muir *et al.* [7].

3.2. MSH mineral mode and crystallinity results

Mount St. Helens dacites comprise plagioclase, orthopyroxene, Fe-Ti oxides, clinopyroxene, apatite and quartz in order of decreasing abundance. Plagioclase and orthopyroxene are much more abundant than the other phases and hornblende occurs only as remnants of reacted phenocrysts.

Total crystallinity of summer 1980 pumices increased from 14 vol% on 25 May 1980 (70 days from an earthquake swarm on 17 March 1980) to 22 vol% in August. This crystallinity increase is dominated by plagioclase which increased from 54 vol% to 74 vol% over the same period. Groundmass plagioclase modal abundance normalised to vesicle- and glass-free area is 74 - 92 vol% in samples erupted May and June 1980 demonstrating the abundance of this phase.

Groundmass crystallinity variations in 1980 to 1986 domes (Fig; 6) are (1) variable (11 – 32 vol%) but increasing at around 8 vol% per month in cryptodome samples between 13 April and 12 June 1980; (2) increasing gradually post-summer 1980 from 39 vol% to 53 vol%. Groundmass crystallinities of cryptodome from 18 May 1980 are similar to pumices erupted summer 1980 (14 - 23 vol%) and lower than post-summer 1980 dome samples probably as cryptodome material experienced shorter residence times in the shallow crust providing scant opportunity for further crystallisation. Cryptodome vesicle fractions range from 1 vol% to 26 vol% but post-summer 1980 domes all have vesicle fractions less than 10 vol%. Phenocryst-free plagioclase modal abundance normalised to vesicle- and glass-free area remains high and similar to summer 1980 samples although it decreases gradually to 64 vol% in May 1986. Over the same period modal orthopyroxene abundance increases from ~10 vol% to ~25 vol%.

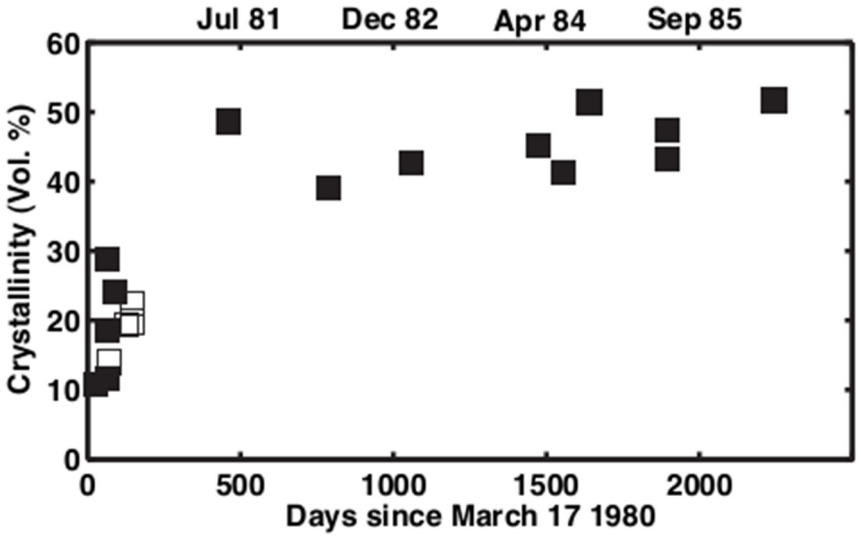

Figure 6. Total groundmass crystallinity of 1980 to 1986 erupted samples. Data are normalised to vesicle-free area. Open symbols are pumices; filled symbols are cryptodomes and domes. Figure from Muir *et al.* [7].

3.3. Interpretation of CSD, crystallinity and mineral mode trends

Variations in magma storage and ascent history for different stages of the 1980 to 1986 Mount St. Helens eruption can be distinguished from CSD, crystallinity and mineral mode data. The observation that post-summer 1980 n^0 and $G\tau$ remain relatively constant over a long time period suggests similar crystallisation kinetics prevailed compared with dome samples erupted during summer 1980. $G\tau$ of orthopyroxene microlites is larger than for plagioclase microlites post-summer 1980. As microlites are the final crystals to form pre- and syn-eruption, we can assume both phases have similar residence times in any given sample. It then follows that orthopyroxene has higher growth rates at shallow depths and ascent rates typical of Mount St. Helens domes.

Nucleation is dominant at highest ΔT, which is expected during rapid ascent rates. Therefore, samples with higher n^0, such as the summer 1980 cryptodome (sample SHKB25) most likely experienced faster decompression during high mass eruption rates with system recharge occurring over relatively short time periods.

If we assume that G is constant throughout the dome-building portion of the eruption it is possible to define a value of τ that results in constant G. Conversely, G can be estimated by taking τ to be the number of days since the 17 March 1980 earthquake swarm until the sample eruption date. Performing this calculation, G is higher in summer 1980 domes than for 1984 to 1986 domes and τ must be increased to the number of days since January 1978 (approximately 800 days before the 18 May 1980 eruption) to maintain a fairly constant G. Values of G calculated using this method for plagioclase microphenocrysts (1.2 to 2.9 $\times$ 10^{-10} mm s^{-1}) are similar to those previously calculated for plagioclase at Mount St. Helens.

4. CONCLUSIONS

Advances in SEM-EDS silicon drift detectors mean X-ray spectral images (XSI) can be acquired faster over larger areas without sacrificing data quality. It is now feasible to use XSI as the basis for textural studies of volcanic rocks in place of more traditional backscattered electron images. A major benefit of using XSI data is that crystallinity and mineral mode data can be obtained at the same time as crystal size data. Crystals, glass (quenched melt) and vesicles can be segmented based on chemical differences to produce binary maps which form the basis of crystal size, shape and area measurements. Applying this method to samples erupted from Mount St Helens, USA during the 1980 to 1986 eruptive episode shows stark differences in crystal textures and total crystallinities between the explosive phase of summer 1980 and the effusive, dome-forming phase post-summer 1980.

5. REFERENCES

[1] Fitzgerald R, Keil K and Heinrich K F J 1968 Solid-state energy-dispersion spectrometer for electron-microprobe X-ray analysis. *Science* **159** 528-530

[2] Newbury D E and Ritchie N W M 2013 Elemental mapping of microstructures by scanning electron microscopy-energy dispersive X-ray spectrometry (SEM-EDS): extraordinary advances with the silicon drift detector (SDD). *J. Anal. At. Spectrom.* **28** 973-988

[3] Winkler H G F 1947 Kristallgrösse und Abkühlung. *Heidelb. Beitr. Mineral. Petrol.* **1** 87-104

[4] Cashman K and Blundy J 2000 Degassing and crystallization of ascending andesite and dacite. *Philos. Trans. R. Soc. Lond. Math. Phys. Eng. Sci.* **358** 1487-1513

[5] Scott W E, Sherrod D R and Gardner C A 2008 Overview of the 2004 to 2006, and continuing, eruption of Mount St. Helens, Washington: Chapter 1 in A volcano rekindled: the renewed eruption of Mount St. Helens, 2004-2006. US Geol. Surv Prof. Pap. 1750-1 (Reston, VA: U.S. Geological Survey)

[6] Endo E T, Dzurisin D and Swanson D A 1990 Geophysical and observational constraints for ascent rates of dacitic magma at Mount St. Helens. in: *Magma transport and storage*. (Ryan M P; Ed.) (New York, NY:: John Wiley & Sons) 318-334

[7] Muir D D, Blundy J D and Rust A C 2012 Multiphase petrography of volcanic rocks using element maps: a method applied to Mount St. Helens, 1980-2005. *Bull. Volcanol.* **74** 1101-1120

[8] Buse B and Kearns S 2018 Evaluating X-ray microanalysis phase maps using principal component analysis. *Microsc. Microanal.* **24** 1-10

[9] Schneider C A, Rasband W S and Eliceiri K W 2012 NIH Image to ImageJ: 25 years of image analysis. *Nature Methods* **9** 671-675

[10] Higgins M D 2000 Measurement of crystal size distributions. *Amer Mineralogist* **85** 1105-1116

[11] Morgan D J and Jerram D A 2006 On estimating crystal shape for crystal size distribution analysis. *J. Volcanol. Geotherm. Res.* **154** 1-7

[12] Marsh B D 1998 On the interpretation of crystal size distributions in magmatic systems. *J. Petrology* **39** 553-599